The Journal of Immunology

RESEARCH ARTICLE | OCTOBER 02 2023

Myeloid Heterogeneity Mediates Acute Exacerbations of Pulmonary Fibrosis

Jennifer L. Larson-Casey; ... et. al

J Immunol (2023) 211 (11): 1714–1724.
https://doi.org/10.4049/jimmunol.2300053

Myeloid Heterogeneity Mediates Acute Exacerbations of Pulmonary Fibrosis

Jennifer L. Larson-Casey,* Komal Saleem,*,[1] Ranu Surolia,*,[1] Jyotsana Pandey,* Matthias Mack,[†] Veena B. Antony,* Sandeep Bodduluri,*,[‡] Surya P. Bhatt,*,[‡] Steven R. Duncan,* and A. Brent Carter*,[§]

Epidemiological evidence indicates that exposure to particulate matter is linked to the development of idiopathic pulmonary fibrosis (IPF) and increases the incidence of acute exacerbations of IPF. In addition to accelerating the rate of lung function decline, exposure to fine particulate matter (particulate matter smaller than 2.5 μm [$PM_{2.5}$]) is a risk factor for increased mortality in subjects with IPF. In this article, we show that exposure to $PM_{2.5}$ mediates monocyte recruitment and fibrotic progression in mice with established fibrosis. In mice with established fibrosis, bronchoalveolar lavage cells showed monocyte/macrophage heterogeneity after exposure to $PM_{2.5}$. These cells had a significant inflammatory and anti-inflammatory signature. The mixed heterogeneity of cells contributed to the proinflammatory and anti-inflammatory response. Although monocyte-derived macrophages were recruited to the lung in bleomycin-injured mice treated with $PM_{2.5}$, recruitment of monocytes expressing Ly6C^{hi} to the lung promoted progression of fibrosis, reduced lung aeration on computed tomography, and impacted lung compliance. Ly6C^{hi} monocytes isolated from $PM_{2.5}$-exposed fibrotic mice showed enhanced expression of proinflammatory markers compared with fibrotic mice exposed to vehicle. Moreover, IPF bronchoalveolar lavage cells treated ex vivo with $PM_{2.5}$ showed an exaggerated inflammatory response. Targeting Ly6C^{hi} monocyte recruitment inhibited fibrotic progression in mice. Moreover, the adoptive transfer of Ly6C^{hi} monocytes exacerbated established fibrosis. These observations suggest that enhanced recruitment of Ly6C^{hi} monocytes with a proinflammatory phenotype mediates acute exacerbations of pulmonary fibrosis, and targeting these cells may provide a potential novel therapeutic target to protect against acute exacerbations of IPF. *The Journal of Immunology*, **2023, 211: 1714–1724.**

Air pollution is the leading environmental cause of premature reversible death and disability in the world (1). The component of air pollution containing particulate matter smaller than 2.5 μm ($PM_{2.5}$) in diameter accounts for most health impacts caused by air pollution. More than 13% of deaths in the United States are attributable to exposure to $PM_{2.5}$ (2). The adverse effects of $PM_{2.5}$ are well established in subjects with cardiovascular disease, hypertension, type 2 diabetes mellitus, chronic kidney disease, chronic obstructive pulmonary disease (COPD), and asthma (1, 3, 4); however, $PM_{2.5}$ has only recently been recognized as a factor in the progression of idiopathic pulmonary fibrosis (IPF) (5, 6).

IPF is characterized by progressive, irreversible scarring of the lungs (7). Approximately 30% of individuals with IPF experience an acute exacerbation (AE), a sudden acceleration of the disease resulting in respiratory failure. AE-IPF results in a median survival of <3 mo (8–11). In addition to accelerating the rate of lung function decline, exposure to $PM_{2.5}$ increases progression and mortality in IPF (12–15). $PM_{2.5}$ exposure leads to adverse clinical outcomes in IPF (12, 13, 15–18); however, critical knowledge gaps exist in the cellular and molecular mechanism(s) that mediate AE-IPF.

Increased circulating monocyte count is associated with poor outcomes in IPF and is a prognostic marker of mortality in subjects with fibrotic diseases (19, 20). In particular, subjects with progressive IPF show higher monocyte counts and a poorer prognosis than those with nonprogressive disease (19, 20). A retrospective study determined that absolute monocyte count was an independent risk factor for AE in individuals with progressive fibrosing interstitial lung disease (21).

In fibrotic disorders of the lung, monocyte-derived macrophages (MDMs) have a decisive role in fibrotic remodeling of the injured lung. We have previously shown that macrophages have an anti-inflammatory phenotype in several models of pulmonary fibrosis,

*Division of Pulmonary, Allergy, and Critical Care Medicine, Department of Medicine, University of Alabama at Birmingham, Birmingham, AL; [†]Department of Nephrology, University of Regensburg, Regensburg, Germany; [‡]UAB Lung Imaging Lab, University of Alabama at Birmingham, Birmingham, AL; and [§]Birmingham Veterans Administration Medical Center, Birmingham, AL

[1]K.S. and R.S. contributed equally to this work.

ORCIDs: 0000-0001-7238-7986 (J.L.L.-C.); 0009-0008-5273-1960 (K.S.); 0000-0002-8418-4497 (S.P.B.); 0000-0001-6002-4715 (A.B.C.).

Received for publication January 20, 2023. Accepted for publication September 15, 2023.

This work was supported by the National Institute of Environmental Health Sciences, National Institutes of Health (Grants 5R01ES015981-15 and P42 ES027723-03 to A.B.C.), U.S. Department of Veteran Affairs (Grant 5I01 CX001715-04 to A.B.C.; Grant U01 HL133232-01A1 to S.R.D.; and Grant R01 HL151421 to S.P.B.), and a University of Alabama at Birmingham Faculty Development Grant (to J.L.L.-C.). Additional support was provided by the Comprehensive Flow Cytometry Core through the Center for AIDS Research (Grant AI027767), the O'Neal Comprehensive Cancer Center (Grant CA013148), and the University of Alabama at Birmingham High Resolution Imaging Facility.

J.L.L.-C. and A.B.C. developed the concept and design of the study. J.L.L.-C., K.S., R.S., and J.P. assisted with conducting experiments. J.L.L.-C., R.S., J.P., S.B., S.P.B., S.R.D., and A.B.C. acquired data. J.L.L.-C., M.M., V.B.A., and A.B.C. provided reagents. J.L.L.-C., M.M., S.B., S.P.B., S.R.D., and A.B.C. provided analysis and interpretation of experiments and results. J.L.L.-C. and A.B.C. wrote the manuscript.

Address correspondence and reprint requests to Dr. Jennifer L. Larson-Casey, 1918 University Boulevard, 710 MCLM, Pulmonary, Allergy, and Critical Care Medicine, University of Alabama at Birmingham, Birmingham, AL 35294. E-mail address: jennifercasey@uabmc.edu

The online version of this article contains supplemental material.

Abbreviations used in this article: AE, acute exacerbation; AE-PF, acute exacerbation of pulmonary fibrosis; BAL, bronchoalveolar lavage; COPD, chronic obstructive pulmonary disease; CT, computed tomography; HU, Hounsfield unit; IPF, idiopathic pulmonary fibrosis; i.t., intratracheally; MDM, macrophage-derived macrophage; MHC II, MHC class II; mtROS, mitochondrial reactive oxygen species; $PM_{2.5}$, particulate matter smaller than 2.5 μm; RAM, resident alveolar macrophage; WT, wild-type.

https://doi.org/10.4049/jimmunol.2300053

including IPF (22–27). The role of distinct subsets of macrophages, including MDMs, has not been determined in AE-IPF. In contrast with IPF, AE-IPF is thought to often be triggered by an acute inflammatory or infectious process (28).

We show that mice with established fibrosis are more susceptible to fibrotic progression after exposure to particulate matter. In our AE of pulmonary fibrosis (AE-PF) mouse model, mice show a combined increase in proinflammatory and anti-inflammatory responses in isolated mononuclear cells. Recruitment of Ly6C monocytes was a component in the population of mononuclear cells. Inhibition of Ly6C^{hi} monocyte recruitment by administration of an mAb to mice prevented fibrotic progression and decreased the inflammatory response in our murine model of AE-PF.

Materials and Methods

Human subjects

We obtained human bronchoalveolar lavage (BAL) cells as previously described (29) from IPF subjects under protocols (300001124 and 01670) approved by the Human Subjects Institutional Review Boards of University of Alabama at Birmingham and the Birmingham Veterans Administration Medical Center, respectively. Human BAL specimens were used for research only. All subjects provided prior written consent to participate in the study. IPF subjects had to meet the following criteria: (1) forced vital capacity at least 50% predicted, (2) current nonsmoker, (3) no recent or current evidence of infection, (4) evidence of restrictive physiology on pulmonary function tests, and (5) usual interstitial pneumonia pattern on high-resolution chest computed tomography (CT). Fiberoptic bronchoscopy with BAL was performed after subjects received local anesthesia. Three subsegments of the lung were lavaged with five 20-ml aliquots of normal saline, and the first aliquot in each was discarded. The percentage of macrophages was determined by Wright–Giemsa stain and varied from 90 to 98%.

Animal studies

Protocols were approved by University of Alabama at Birmingham Institutional Animal Care and Use Committee under protocol 22294 and were performed in accordance with National Institutes of Health guidelines. Eight- to twelve-week-old male and female wild-type (WT) C57BL/6J mice were intratracheally (i.t.) administered 1.75 U/kg bleomycin or saline as a negative control. On day 14 or 21, mice were exposed to vehicle (saline) or 8.25 μg $PM_{2.5}$ [equivalent human dose to the maximal Environmental Protection Agency daily standard, 35 μg/m^3 (30)] i.t. daily for 7 consecutive days. BAL was performed at 21 or 28 d. In some experiments mice were treated with an anti-CCR2 mAb, clone MC-21 (20 μg i.p. daily), or IgG control for 5 d, as previously described (31). For adoptive transfer studies, 1×10^6 bone marrow–derived, FACS-sorted Ly6C^{hi} monocytes or media were administered i.t. Adoptive transfer was performed 1 d before bleomycin exposure with mice harvested on day 21, or 21 d after bleomycin exposure with mice harvested on day 28. BAL was conducted and cytospins were generated to determine cell differential by Wright–Giemsa stain. The lungs were removed and stained for collagen using Masson's trichrome staining. Blood monocytes were isolated from cardiac puncture by density gradient centrifugation using Ficoll-Paque. Bone marrow cells were isolated from the femurs and tibias of WT mice.

Micro-CT imaging

Under isoflurane anesthesia, in vivo micro-CT images were acquired (MILabs small animal micro-CT) in supine position at deep inspiratory phase of respiration. The following image parameters were used for the image acquisition at tube voltage (55 kV) and tube current (0.19 mA) and with 20-ms exposure. After image acquisition, the lung parenchyma was segmented using Otsu algorithm provided by Chest Imaging Platform package in 3D-Slicer imaging software (32). The density threshold for lung parenchyma was automatically selected through Otsu algorithm to separate regions of lung parenchyma. The generated lung mask was subsequently used to identify regions higher and lower than −500 Hounsfield units (HUs) representing nonaerated and aerated lung regions (33).

Respiratory mechanics analysis

Anesthetized mice (xylazine, 5 mg/kg and ketamine, 130 mg/kg) were subjected to FlexiVent (SCIREO, Montreal, QC, Canada), as previously described (34). In brief, tracheotomy was performed for intubation. Mice were mechanically ventilated at 150 breaths/min, tidal volume of 10 ml/kg, and a positive end expiratory pressure of 3 cmH_2O. Compliance was evaluated using the PV-Loop Salazar Knowles equation. Investigators were blinded to treatment conditions during experiments and when assessing the outcome.

Quantitative real time PCR

Total RNA was isolated and reverse transcribed, and quantitative real-time PCR was performed as described previously (23). Data were calculated by the cycle threshold ($^{\Delta\Delta}$CT) method, normalized to β-actin, and expressed in arbitrary units. The following primer sets were used: mouse Arginase 1 RNA, mouse arginase I: 5′-CAG AAG AAT GGA AGA GTC AG-3′ and 5′-CAG ATA TGC AGG GAG TCA CC-3′; mouse TGF-β1: 5′-CGG AGA GCC CTG GAT ACC A-3′ and 5′-TGC CGC ACA CAG CAG TTC-3; mouse Ly6C: 5′-CTG CAG TGC TAC GAG TGC TA-3′ and 5′-TGC AGA ATC CAT CAG AGG CG-3′; mouse TNF-α: 5′-CAC TTG GTG GTT TGC TAC GA-3′ and 5′-CCA CAT CTC CCT CCA GAA AA-3′; human Arginase-1: 5′-TTC TCA AAG GGA CAG CCA CG-3′ and 5′-TAG GGA TGT CAG CAA AGG GC-3′; human iNOS: 5′-CGG TGC TGT ATT TCC TTA CGA GGC GAA GAA GG-3′ and 5′-GGT GCT GCT TGT TAG GAG GTC AAG TAA AGG GC-3′; human TGF-β1: 5′-CGT GGA GCT GTA CCA GAA ATA C-3′ and 5′-CAC AAC TCC GGT GAC ATC AA-3′; human TNF-α: 5′-CAG CCT CTT CTC CTT CCT GA-3′ and 5′-AGC CTT GGC CCT TGA AGA-3′.

Flow cytometry

Cells were blocked with 1% BSA containing TruStain fcX (anti-mouse CD16/32) Ab (101319; BioLegend), followed by staining with Abs. Abs used were Rat anti-mouse CD45-PE (12-0451-82; eBioscience), LIVE Dead-eFlour506 (65-0866; Invitrogen), Rat anti-mouse CD11b-allophycocyanin-Cy7 (101225; BioLegend), anti-mouse CD64-PE-Cy7 (139313; BioLegend), Rat anti-mouse Ly6G-AF700 (561236; BD), Rat anti-mouse Siglec F-allophycocyanin (155507; BioLegend), Rat anti-mouse Ly6C: eFlour450 (48-5932-82; Invitrogen), and Rat anti-mouse MHC class II (MHC II)-PerCP-Cy5.5 (562363; BD). A hierarchical gating strategy was used to represent resident alveolar macrophages (RAMs) as CD45$^+$CD11b$^{+/-}$Ly6G$^-$CD64$^+$Ly6C$^-$Siglec F^{hi}; MDMs as CD45$^+$CD11b$^{+/-}$Ly6G$^-$CD64$^+$Ly6C$^-$Siglec F^{lo}; Ly6C^{hi} as CD45$^+$CD11b$^+$Ly6G$^-$CD64$^{+/-}$MHC II$^-$Ly6C^{hi}Siglec F$^-$; Ly6C^{lo} as CD45$^+$CD11b$^+$Ly6G$^-$CD64$^{+/-}$MHC II$^-$Ly6C^{lo}Siglec F$^-$; and Ly6C^{hi} bone marrow–derived monocytes and blood monocytes as CD45$^+$CD11b$^+$Ly6G$^-$Ly6C^{hi}. Data were acquired on FACSAria II, LSR Fortessa, or LSR II (BD Biosciences) using BD FACSDiva software (version 8.0.1). Data were analyzed using FlowJo (FlowJo) software (Version 10.5.0).

Confocal imaging

BAL cells were fixed with 4% paraformaldehyde in PBS for 45 min at room temperature, followed by permeabilization for 3 min and incubated with PBS containing 5% BSA for 45 min. Cells were incubated with rat anti–Ly6C-FITC (ab25025; Abcam) and counterstained with DAPI. Nikon A1 Confocal was used for imaging.

Immunohistochemistry

The immunohistochemistry protocol was previously described (22). In brief, lung tissue sections from mouse (4 μm thick) were prepared and deparaffinized. Tissues were rehydrated with gradient series of ethanol followed by blocking and incubated with TruStain FcX PLUS anti-mouse CD16/32 (156604; BioLegend). All the sections were stained with ZO-1 anti-rabbit polyclonal (61-7300; Thermo Fisher), Goat Anti-Rabbit IgG (H+L), Mouse/Human ads-TRITC (4050-031; Southern Biotech), and then counterstained with DAPI (MP Biologicals). Tissue sections were fixed using Vecta Mount, permanent mounting medium (Vector Laboratories) followed by confocal microscopy. The Nikon A1 confocal microscope was used for imaging.

ELISA

Active TGF-β1, TNF-α, and CCL2 expression were determined in BALF using ELISA kits (R&D Systems) according to the manufacturer's instructions. Mouse albumin ELISA was determined as previously described (23).

Hydroxyproline analysis

Lung tissues were dried to a stable weight and acid hydrolyzed with 6N HCl for 24 h at 110°C. Samples were resuspended in 1.5 ml PBS followed by incubation at 60°C for 1 h. Samples were centrifuged at 13,000 rpm, and the supernatant was taken for hydroxyproline analysis by using chloramine-T. Hydroxyproline concentration was normalized to the dry weight of the tissue (23).

Mitochondrial ROS generation

MitoSOX, a mitochondrial superoxide indicator (Thermo Fisher Scientific), was used to detect mitochondrial superoxide anion according to the manufacturer's protocol. Equal numbers of cells were treated with 5 μM for 30 min at 37°C and subjected to fluorescent reading (excitation, 510 nm; emission, 580 nm).

Materials

Bleomycin was obtained from the University of Alabama at Birmingham Animal Resources Program. $PM_{2.5}$ was collected from ambient air in an urban area and purchased from National Institute of Standards and Technology standard reference material.

Statistics

Statistical comparisons were performed using a Student *t* test when only two groups of data are presented, or one-way ANOVA with a Tukey's post hoc test. All results were expressed as mean ± SEM, and $p < 0.05$ was considered to be significant. GraphPad Prism statistical software was used for all analyses.

Study approval

We obtained BAL cells under approved protocols 300001124 and 01670 by the Human Subjects Institutional Review Board of the University of Alabama at Birmingham and the Birmingham Veterans Administration Medical Center, respectively. Human BAL specimens were used for research only. All subjects provided prior written consent to participate in the study. Animal experiments were approved by the University of Alabama at Birmingham Institutional Animal Care and Use Committee under protocol 22294 and were performed in accordance with National Institutes of Health guidelines.

Results

Fibrotic progression occurs in AE-PFs

Recent epidemiological evidence indicates that $PM_{2.5}$ can cause AE-IPF (15, 35). To determine whether fibrotic progression occurred in an early stage of fibrosis (36), we subjected mice to daily exposure of $PM_{2.5}$ starting on day 14 after bleomycin exposure. On day 21, histology revealed that bleomycin exposure led to increased collagen deposition in the lungs compared with mice receiving saline (Fig. 1A). Mice exposed to $PM_{2.5}$ showed evidence of inflammation compared with vehicle-exposed mice, whereas mice exposed to $PM_{2.5}$ in early established fibrosis showed similar collagen deposition to mice that received vehicle (Fig. 1B).

Because increased circulating monocyte count is a prognostic marker of mortality in patients with fibrotic diseases (19, 20), we determined whether monocyte recruitment was involved in $PM_{2.5}$-mediated AE-PF. Although monocytic cells were the predominant cell type in the BAL (>90%) from control and fibrotic mice exposed to vehicle or $PM_{2.5}$ (Fig. 1C), the number of BAL cells in fibrotic mice exposed to $PM_{2.5}$ was not significantly different from bleomycin-injured mice exposed to vehicle (Fig. 1D). There was also no difference in survival throughout the 21 d in the mice that received bleomycin (Fig. 1E).

Data indicate that AEs occur in individuals with advanced interstitial lung disease (8). We questioned whether $PM_{2.5}$ mediated fibrotic progression in mice with greater established fibrosis. At 21 d after mice were exposed to saline or bleomycin, mice received daily exposure to vehicle or $PM_{2.5}$ for 7 consecutive days. On day 28, collagen deposition was detected in the lungs of bleomycin-exposed mice (Fig. 1F); however, mice exposed to $PM_{2.5}$ with established fibrosis showed further architecture destruction and widespread collagen deposition. These results were confirmed biochemically with hydroxyproline analysis (Fig. 1G). Monocytic cells were the predominant cell type in the BAL regardless of exposure (Fig. 1H), and the number of cells in the BAL was significantly increased in mice exposed to $PM_{2.5}$ compared with bleomycin-exposed mice receiving vehicle (Fig. 1I). Fibrotic mice that received $PM_{2.5}$ beginning on day 21 showed a significant reduction in survival compared with fibrotic mice receiving vehicle (Fig. 1J). These data suggest $PM_{2.5}$ mediates fibrotic progression in mice with more advanced established fibrosis.

BAL cells in mice have a mixed phenotype in AE-PF

Although monocytic cells are critical in initiating an innate immune response to injury, they are also involved in tissue repair responses. Macrophages are highly plastic and polarize to a predominant phenotype in response to environmental stimuli (22, 23, 37). Because macrophages have an anti-inflammatory phenotype in several models of pulmonary fibrosis, we questioned whether macrophage/monocyte polarization regulated fibrotic progression in our mouse model of AE-PF. $PM_{2.5}$ exposure induced a proinflammatory phenotype in BAL cells with increased *Tnf* and *Nos2* mRNA expression (Fig. 2A, 2B), whereas BAL cells from bleomycin-injured mice had a reduction in proinflammatory markers below the saline control. The anti-inflammatory genes, *Tgfb1* and *Arg1*, were increased after bleomycin (Fig. 2C, 2D), whereas exposure to $PM_{2.5}$ led to a greater increase in these anti-inflammatory genes compared with bleomycin-injured mice.

Exposure to $PM_{2.5}$ increased the inflammatory microenvironment in the lung. TNF-α levels in BAL fluid were significantly increased in mice that had AE-PF compared with bleomycin-injured mice (Fig. 2E). In addition, active TGF-β1 levels were increased further in the BAL fluid from mice with established fibrosis that received $PM_{2.5}$ compared with fibrotic mice (Fig. 2F). These data suggest that BAL cells have a mixed phenotype in a murine model of AE-PF that may contribute to the enhanced fibrotic remodeling seen in these mice.

Evidence indicates that anti-inflammatory cytokines are expressed in pulmonary fibrosis, and lung macrophages from IPF subjects polarize to an anti-inflammatory phenotype (22, 23, 27, 38). To understand the role of macrophage/monocyte phenotype in our model of AE-PF, IPF BAL cells exposed ex vivo to $PM_{2.5}$ showed a significant increase in *TNF* and *NOS2* expression (Fig. 2G, 2H). Potentially due to the predominance of MDMs in IPF BAL (25, 39), *TGFB1* and *ARG1* levels remained unchanged in $PM_{2.5}$-exposed IPF BAL cells (Fig. 2I, 2J). These observations suggest that $PM_{2.5}$ exposure promoted an inflammatory phenotype in IPF BAL cells.

Recruitment of Ly6C-expressing monocytes in AE-PF

Evidence indicates that MDMs are required for fibrotic remodeling in IPF (22, 36, 39). To investigate the role of MDMs within $PM_{2.5}$-mediated AE-PF, we subjected BAL cells from exposed mice to FACS analysis (Supplemental Fig. 1). Bleomycin-induced injury significantly increased MDMs compared with saline. MDM recruitment was similar in bleomycin-injured mice receiving $PM_{2.5}$ (Fig. 3A, 3B). Mice receiving bleomycin showed a significant reduction in the number of RAMs. $PM_{2.5}$ exposure in mice receiving saline did not alter RAM or MDM numbers compared with vehicle. The increase in MDMs in bleomycin-injured mice correlated with greater CCL2 levels in BAL fluid (Fig. 3C). Interestingly, $PM_{2.5}$-exposed mice receiving saline showed elevated CCL2 similar to bleomycin-injured mice that received vehicle, whereas CCL2 was further increased in bleomycin-injured mice with AE-PF even though numbers of MDMs were unchanged.

Because mice with AE-PF had increased cellular recruitment and CCL2 levels, we investigated the role of the two major subsets of murine monocytes, Ly6C^{hi} (classical monocytes) and Ly6C^{lo} (nonclassical). Ly6C^{hi} monocytes are recruited from the bone marrow and accumulate at sites of injury and inflammation, whereas Ly6C^{lo} monocytes are involved in early inflammatory responses (40). Confocal analysis in BAL cells showed Ly6C staining was increased to a greater extent in fibrotic mice with AE-PF (Fig. 3D, 3E). These results contrasted with vehicle-exposed mice that had an absence of Ly6C staining.

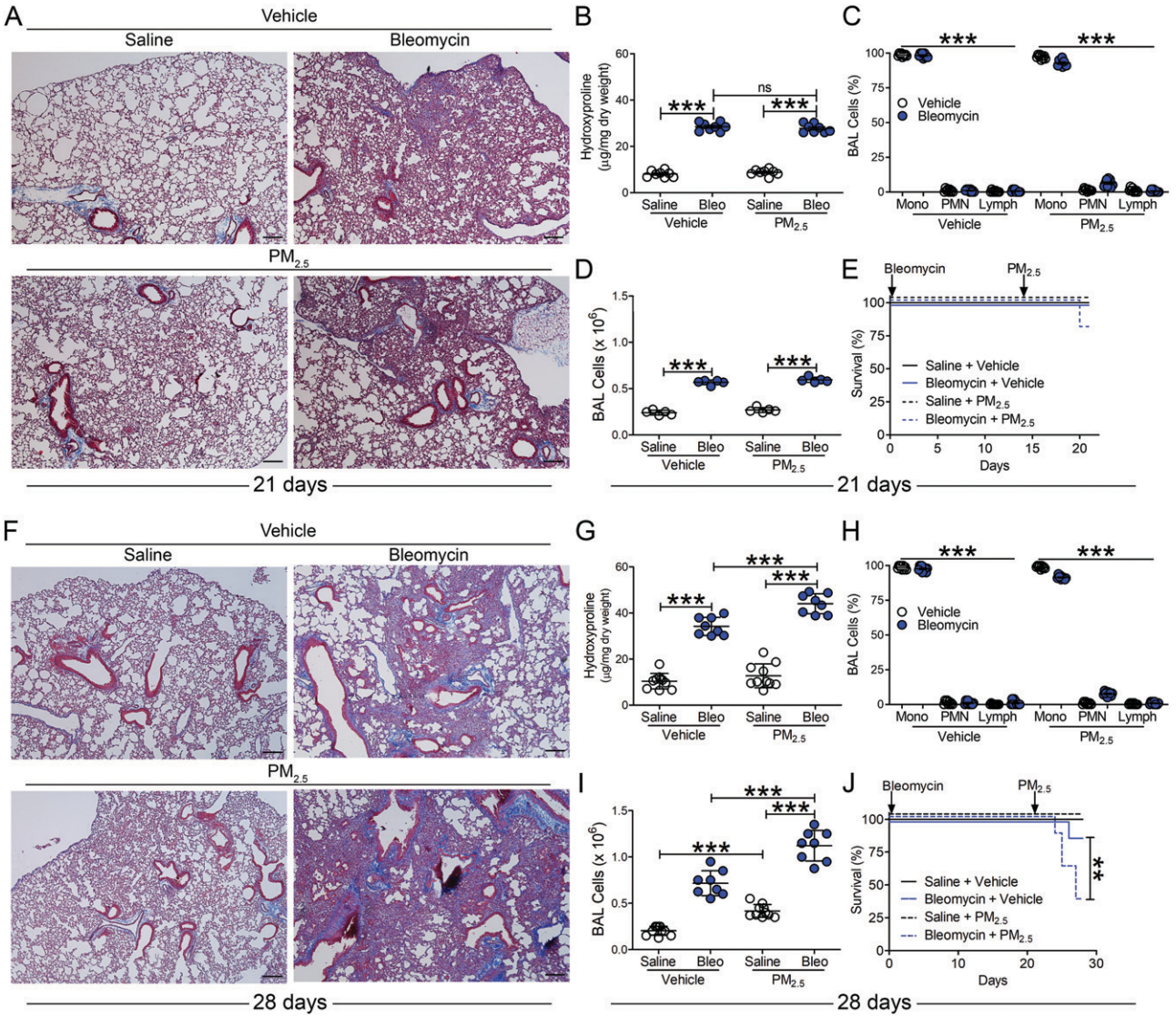

FIGURE 1. Fibrotic progression occurs in AE-PF. WT mice were exposed to saline or bleomycin (Bleo; 1.75 U/kg i.t.). At day 14, mice were exposed to saline (vehicle) or $PM_{2.5}$ (8.25 μg in saline, i.t.) daily. Lungs were excised and BAL was performed on day 21. (**A**) Representative Masson's trichrome staining of lung tissues. $n = 8$. Scale bars, 200 μm. (**B**) Hydroxyproline analysis of lung homogenates. $n = 8$. (**C**) Cell differential using Wright–Giemsa stain to identify mononuclear (mono), neutrophil (PMN), and lymphocytes (lymph). $n = 9$. (**D**) Total number of BAL cells. $n = 5$. (**E**) Kaplan–Meier survival curve. $n = 5$. WT mice were exposed to saline or bleomycin. At day 21, mice were exposed to vehicle or $PM_{2.5}$ daily. Lungs were excised, and BAL was performed on day 28. (**F**) Representative Masson's trichrome staining of lung tissues. $n = 5$. Scale bars, 200 μm. (**G**) Hydroxyproline analysis of lung homogenates. $n = 8$–10. (**H**) Cell differential of BAL cells. $n = 9$–10. (**I**) Total number of BAL cells. $n = 8$–10. (**J**) Kaplan–Meier survival curve. $n = 8$. Values shown represent means ± SEM. One-way ANOVA followed by Tukey's multiple comparison test was used for (B–D) and (G–I), and a log-rank (Mantel–Cox) test was used for (E) and (J). Data shown were pooled from three independent experiments. $^{**}p < 0.001$, $^{***}p < 0.0001$.

Determining the contribution of each monocyte subset, BAL cells subjected to FACS analysis showed an absence of $Ly6C^{hi}$ and $Ly6C^{lo}$ monocytes in vehicle-exposed mice regardless of receiving saline or bleomycin (Fig. 3F, 3G). The exposure of mice to $PM_{2.5}$ led to the emergence of $Ly6C^{hi}$ and $Ly6C^{lo}$ monocytes, and the number in each subset was significantly increased in $PM_{2.5}$-exposed mice with established fibrosis. Although the number of $Ly6C^{hi}$ monocytes was greater than $Ly6C^{lo}$ monocytes, the number of $Ly6C^{hi}$ monocytes increased further in mice with established fibrosis.

To further investigate Ly6C monocyte recruitment to the lung after $PM_{2.5}$ exposure, we harvested bleomycin-exposed mice 1, 4, and 7 d after $PM_{2.5}$ exposure. Recruitment of $Ly6C^{hi}$ monocytes was apparent 1 d after $PM_{2.5}$ exposure, and the number of $Ly6C^{hi}$ monocytes increased significantly in a time-dependent manner (Fig. 3H). A similar increase was seen in the number of $Ly6C^{lo}$ monocytes, although the number of $Ly6C^{lo}$ monocytes was markedly less than $Ly6C^{hi}$ monocytes.

Because Ly6C monocytes were identified in the BAL, lung tissue sections were analyzed for loss of epithelial barrier integrity. Compared with mice receiving vehicle, $PM_{2.5}$-exposed mice showed reduced tight junction protein, ZO-1, as well as punctate staining, suggesting a loss of tight junction barrier of the alveolar epithelium (Fig. 3I, 3J). Moreover, $PM_{2.5}$-exposed mice that received saline had increased albumin in the BAL compared with bleomycin-injured mice. Mice with AE-PF showed significantly greater levels of albumin in the BAL than $PM_{2.5}$-exposed mice (Fig. 3K). In aggregate, these data demonstrate that there is continuous recruitment of Ly6C-expressing monocytes, and there are increased numbers of $Ly6C^{hi}$ and $Ly6C^{lo}$ monocytes in the BAL because of greater loss of barrier integrity in AE-PF.

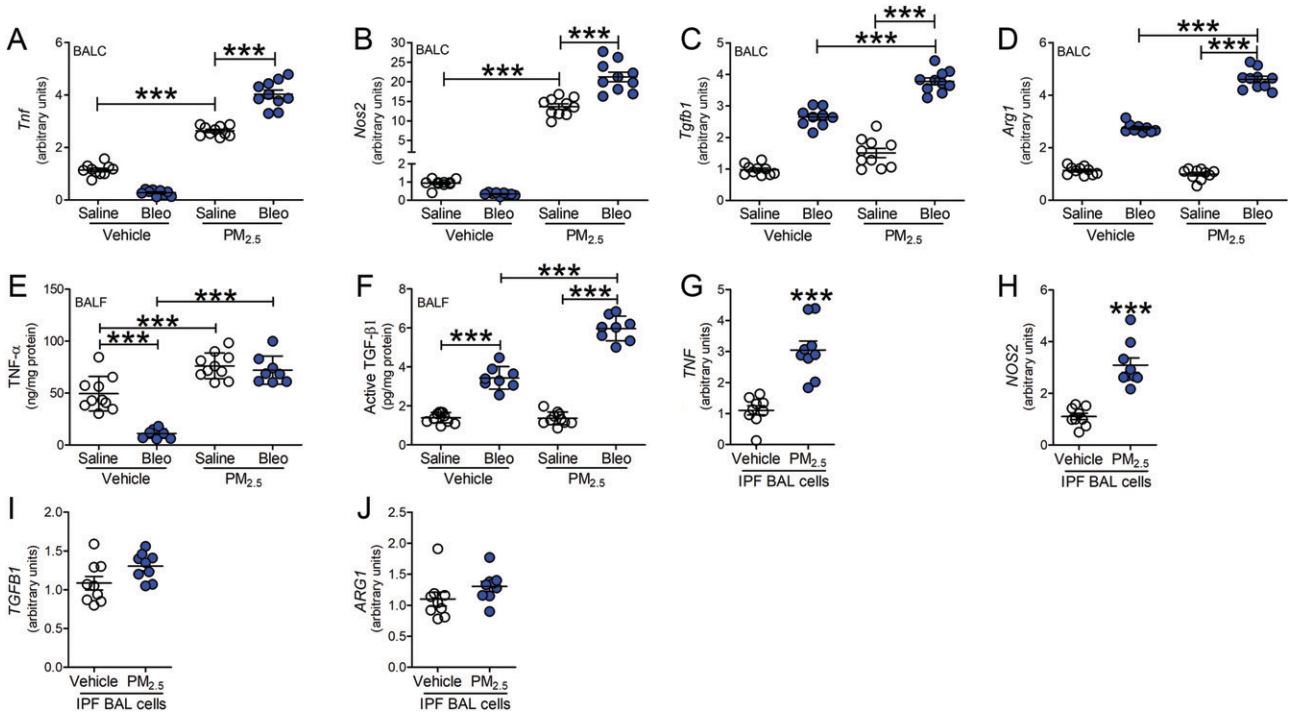

FIGURE 2. BAL cells in mice have a mixed phenotype in AE-PF. WT mice were exposed to saline or bleomycin. At day 21, mice were exposed to vehicle or $PM_{2.5}$ daily. BAL was performed on day 28. mRNA expression for (**A**) *Tnf*, (**B**) *Nos2*, (**C**) *Tgfb1*, and (**D**) *Arg1* in BAL cells. $n = 9–10$. (**E**) TNF-α and (**F**) active TGF-β1 levels in BAL fluid. $n = 8–10$. IPF BAL cells were obtained by BAL and exposed ex vivo to $PM_{2.5}$ (10 μg/cm^2). mRNA expression of (**G**) *TNF*, (**H**) *NOS2*, (**I**) *TGFB1*, and (**J**) *ARG1* levels in BAL cells. $n = 9$. Values shown represent means ± SEM. One-way ANOVA followed by Tukey's multiple comparison test was used for (A–F). Two-tailed *t* test statistical analysis was used for (G–J). Data shown were pooled from three independent experiments. ***$p < 0.0001$.

$PM_{2.5}$ induces recruitment of inflammatory Ly6C^{hi} monocytes to mediate AE-PF

To understand the involvement of macrophage/monocyte subsets in our murine model of AE-PF, FACS-sorted RAMs showed elevated expression of *Tnf* and *Nos2* that remained stable regardless of exposure compared with the reduced expression in MDMs (Fig. 4A–C). Bleomycin-induced injury increased *Tgfb1* and *Arg1* mRNA expression in MDMs; however, these levels were not increased further in mice with AE-PF (Fig. 4A, 4D, 4E).

The sorted Ly6C^{hi} and Ly6C^{lo} monocytes showed prominent phenotypic signatures after $PM_{2.5}$ exposure. The proinflammatory phenotype was markedly increased in Ly6C^{hi} monocytes with elevated *Tnf* and *Nos2* mRNA expression that increased to nearly 15-fold and 6-fold greater in mice with established fibrosis exposed to $PM_{2.5}$ (Fig. 4F–H). In contrast, sorted Ly6C^{lo} monocytes were anti-inflammatory in $PM_{2.5}$-exposed mice with increased *Tgfb1* and *Arg1* expression that were significantly increased in mice with established fibrosis (Fig. 4F, 4I, 4J).

The recruitment of Ly6C^{hi} monocytes into the lung of mice with established fibrosis correlated with enhanced fibrotic remodeling on lung imaging. Micro-CT imaging of lungs at 28 d after bleomycin exposure showed increased tissue density consistent with fibrosis that was not present in saline-exposed mice receiving vehicle or $PM_{2.5}$ (Fig. 4K). Mice with established fibrosis that were administered $PM_{2.5}$ showed evidence of fibrosis with increased lung tissue density. These results were confirmed using −500 HUs to discriminate between aerated (green) and nonaerated lung tissue (red). Although HUs were unchanged in mice exposed to saline, mice with established fibrosis that received vehicle showed an increase in HUs that was further increased in fibrotic mice exposed to $PM_{2.5}$ (Fig. 4L). Bleomycin-exposed mice had a reduction in the percentage of aerated lung tissue, and exposure to $PM_{2.5}$ in mice with established fibrosis showed further reduction in lung aeration (Fig. 4M). Taken together, these results indicate that Ly6C monocytes have both proinflammatory and anti-inflammatory phenotypes that are associated with fibrotic progression to mediate AE-PF in mice.

The generation of mitochondrial reactive oxygen species (mtROS) play a critical role in lung injury and fibrosis (22, 23, 29). Although BAL cells isolated from fibrotic mice exposed to vehicle showed augmented superoxide generation, mice with AE-PF had significantly increased mtROS (Fig. 4N). BAL cells isolated from saline-exposed mice that received $PM_{2.5}$ also showed elevated mtROS levels compared with saline-exposed receiving vehicle. To identify whether Ly6C^{hi} monocytes contributed to mtROS, FACS-sorted Ly6C^{hi} monocytes exposed to $PM_{2.5}$ showed increased superoxide generation (Fig. 4O). Metals are a component of $PM_{2.5}$, and metals often induce mtROS (41, 42). Ly6C^{hi} monocytes treated with the chelating agent, EDTA, showed reduced mtROS levels to that seen in the vehicle control, suggesting, at least in part, that metals in $PM_{2.5}$ contribute to mtROS.

Ly6C^{hi} monocytes mediate fibrotic progression in mice with established fibrosis

To validate that Ly6C^{hi} monocytes are critical in mediating fibrotic progression, we performed adoptive transfer of FACS-sorted progenitor Ly6C^{hi} monocytes into WT mice i.t. Mice were exposed to bleomycin the following day, and BAL was performed 21 d after exposure (Supplemental Fig. 2A). No difference was detected in the number of cells in mice that had the adoptive transfer compared with saline (Supplemental Fig. 2B). Similar expression of inflammatory and anti-inflammatory markers was seen in isolated BAL cells from mice that received Ly6C^{hi} monocytes or saline before bleomycin exposure (Supplemental Fig. 2C–F). There was no difference in

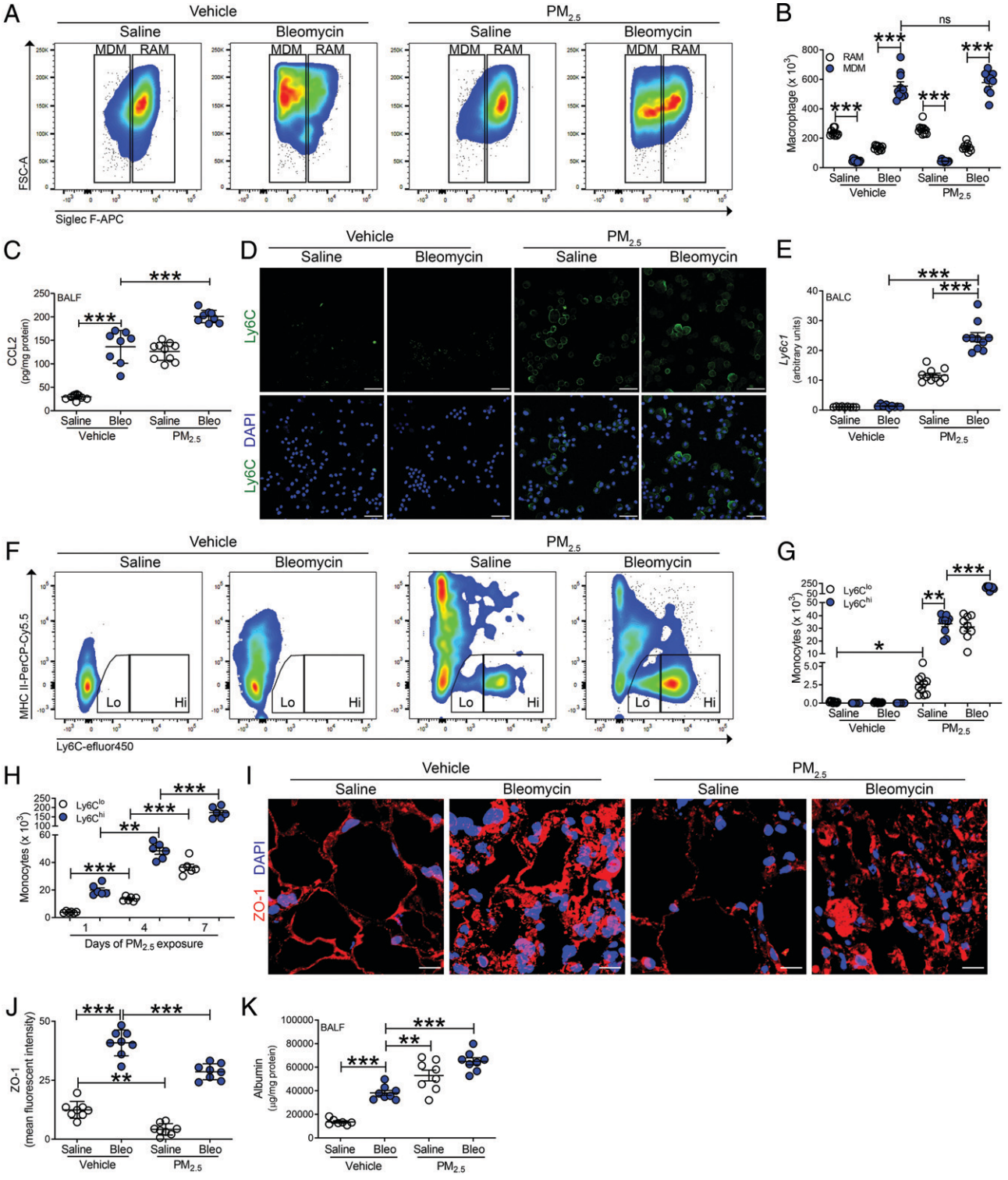

FIGURE 3. Recruitment of Ly6C-expressing monocytes in AE-PF. WT mice were exposed to saline or bleomycin. At day 21, mice were exposed to vehicle or $PM_{2.5}$ daily. BAL was performed on day 28. (**A**) Representative flow cytometry plots of RAMs ($CD45^+CD11b^{+/-}Ly6G^-CD64^+Ly6C^-Siglec\ F^{hi}$) and MDMs ($CD45^+CD11b^{+/-}Ly6G^-CD64^+Ly6C^-Siglec\ F^{low}$). (**B**) Total cell number of RAMs and MDMs from BAL. $n = 9–10$. (**C**) CCL2 levels in BAL fluid. $n = 8–10$. (**D**) Representative confocal images of Ly6C-positive BAL cells counterstained with DAPI. Scale bars, 50 μm ($n = 5$). (**E**) mRNA expression of *Ly6c1* in isolated BAL cells. $n = 9–10$. (**F**) Representative flow cytometry plots of $Ly6C^{lo}$ ($CD45^+CD11b^+Ly6G^-CD64^{+/-}MHC\ II^-Ly6C^{lo}Siglec\ F^-$) and $Ly6C^{hi}$ ($CD45^+CD11b^+Ly6G^-CD64^{+/-}MHC\ II^-Ly6C^{hi}Siglec\ F^-$) monocytes. (**G**) Total cell number of $Ly6C^{lo}$ and $Ly6C^{hi}$ monocytes from BAL. $n = 9–10$. Data shown were pooled from three independent experiments. (**H**) Number of $Ly6C^{lo}$ and $Ly6C^{hi}$ monocytes from BAL in bleomycin-injured mice exposed to $PM_{2.5}$ for indicated days. $n = 6$. (**I**) Representative confocal images of ZO-1 and DAPI staining in mouse lung tissue. Scale bars, 10 μm ($n = 5$). (**J**) Mean fluorescent intensity of ZO-1 staining in lung tissue. $n = 8$. (**K**) Albumin levels in BAL fluid. $n = 7–8$. Data shown are representative from three independent experiments. Values shown represent means ± SEM. One-way ANOVA followed by Tukey's multiple comparison test was used. ns, not significant. $^*p < 0.05$, $^{**}p < 0.001$, $^{***}p < 0.0001$.

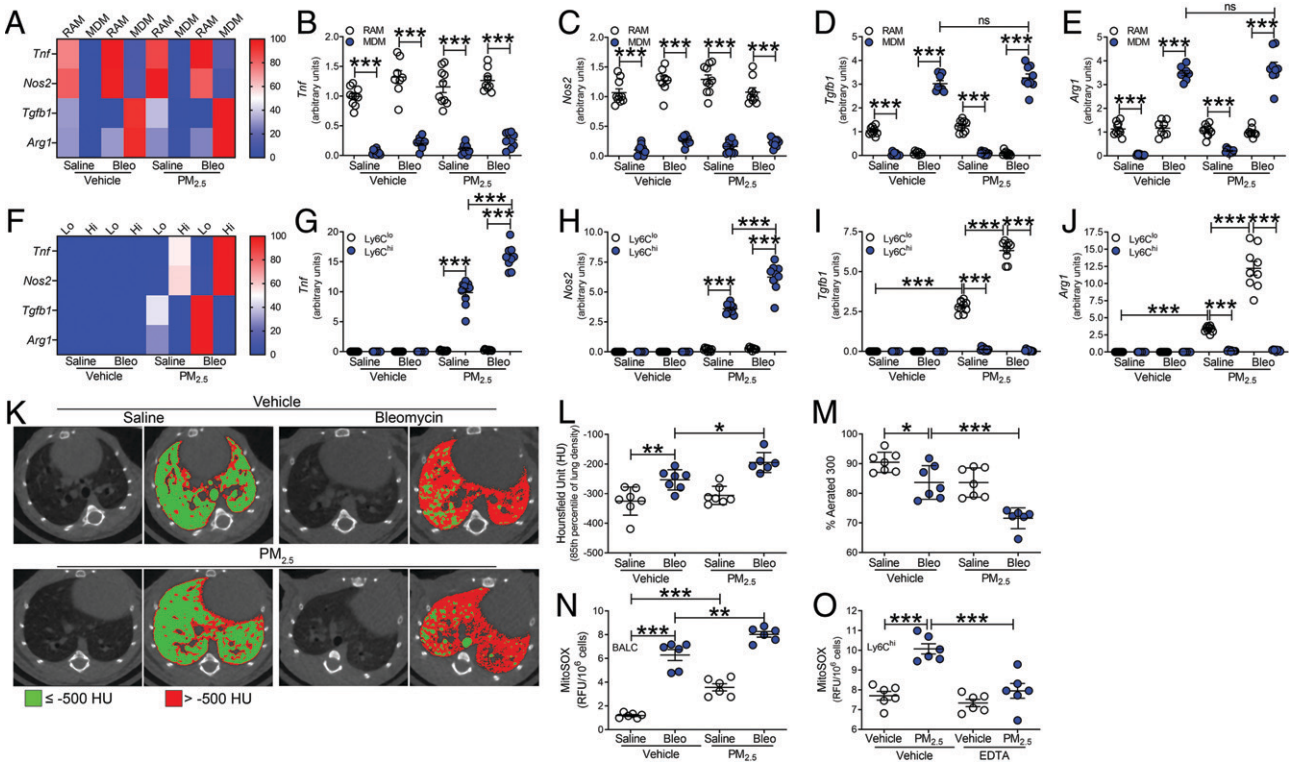

FIGURE 4. $PM_{2.5}$ induces recruitment of inflammatory Ly6C^{hi} monocytes to mediate AE-PF. WT mice were exposed to saline or bleomycin. At day 21, mice were exposed to vehicle or $PM_{2.5}$ daily. BAL was performed on day 28. (**A**) Heatmap of mRNA expression of FACS-sorted RAMs and MDMs for (**B**) *Tnf*, (**C**) *Nos2*, (**D**) *Tgfb1*, and (**E**) *Arg1*. $n = 8–10$. (**F**) Heatmap of mRNA expression of FACS-sorted Ly6C^{lo} and Ly6C^{hi} monocytes for (**G**) *Tnf*, (**H**) *Nos2*, (**I**) *Tgfb1*, and (**J**) *Arg1*. $n = 9–10$. Data shown were pooled from three independent experiments. (**K**) Representative micro-CT images of mouse lung parenchyma identifying ≤−500 HUs (green, aerated lung) and >−500 HUs (red, nonaerated lung) using 3D-Slicer imaging software. Quantification of lung density in (**L**) HUs and (**M**) percentage of aerated lung tissue. $n = 6–7$. Data shown were pooled from two independent experiments. mtROS generation measured by MitoSOX in (**N**) isolated BAL cells from exposed mice ($n = 6$) and (**O**) FACS-sorted Ly6C^{hi} monocytes from bone marrow exposed to $PM_{2.5}$ (10 μg/cm^2) and treated with EDTA (5 mM). $n = 6$. Data shown are representative from three independent experiments. Values shown represent means ± SEM. One-way ANOVA followed by Tukey's multiple comparison test was used. $*p < 0.05$, $**p < 0.001$, $***p < 0.0001$. ns, not significant.

the degree of fibrosis in the mice that received bleomycin (Supplemental Fig. 2G, 2H).

Because AEs occur in patients with advanced interstitial lung disease (8) and our data indicate that $PM_{2.5}$ mediates recruitment of Ly6C^{hi} monocytes to promote fibrotic progression in mice with established fibrosis, we performed an adoptive transfer of Ly6C^{hi} monocytes into mice 21 d after exposure to bleomycin (Fig. 5A). Mice receiving Ly6C^{hi} monocytes had nearly a 2-fold increase in BAL cell number compared with mice that received saline (Fig. 5B). The BAL cells showed heterogeneity with increased inflammatory genes, *Tnf* and *Nos2* (Fig. 5C, 5D), and anti-inflammatory genes, *Tgfb1* and *Arg1* (Fig. 5E, 5F), in fibrotic mice with the adoptive transfer of Ly6C^{hi} monocytes. To determine whether the adoptive transfer of Ly6C^{hi} monocytes regulates fibrotic progression, we excised lungs, which showed widespread collagen deposition and destruction of lung architecture in mice that received Ly6C^{hi} monocytes (Fig. 5G). These results were confirmed by hydroxyproline analysis (Fig. 5H). These data indicate Ly6C^{hi} monocytes do not play a role in fibrotic initiation but rather regulate fibrotic progression after fibrosis is established.

Ly6C^{hi} monocytes are required for AE-PF

Because exposure to $PM_{2.5}$ increased recruitment of Ly6C^{hi} monocytes, we targeted recruited Ly6C^{hi} monocytes in vivo. On day 21 after exposure to saline or bleomycin, mice were exposed to vehicle or $PM_{2.5}$ daily. Mice were treated with an anti-CCR2 mAb, clone MC-21, or IgG control daily beginning on day 23. As expected, at day 28, bleomycin exposure had increased the number of MDMs, and $PM_{2.5}$ exposure did not alter the number of RAMs or MDMs in IgG-treated mice (Fig. 6A, Supplemental Fig. 3A). Although RAM numbers were unaffected in mice treated with the anti-CCR2 compared with IgG, the number of MDMs was reduced in bleomycin-exposed mice. Compared with IgG-treated mice, mice receiving the anti-CCR2 Ab showed nearly complete absence of Ly6C^{hi} monocytes in mice exposed to $PM_{2.5}$ (Fig. 6B, 6C). Treatment with anti-CCR2 did not alter recruitment of Ly6C^{lo} monocytes.

Treatment of mice with the IgG control Ab led to increased *Tnf* and *Nos2* expression in $PM_{2.5}$-exposed mice, whereas the absence of Ly6C^{hi} monocytes in anti-CCR2–treated mice significantly inhibited *Tnf* and *Nos2* mRNA expression in mice receiving $PM_{2.5}$ (Fig. 6D, 6E). Compared with control mice, anti-CCR2–treated mice showed a significant reduction in *Tgfb1* and *Arg1* levels in fibrotic mice exposed to $PM_{2.5}$ (Fig. 6F, 6G). No difference in *Tgfb1* and *Arg1* levels was seen in saline-exposed mice receiving IgG or anti-CCR2. In addition, the inflammatory cytokine TNF-α was significantly reduced in the BAL fluid from $PM_{2.5}$-exposed mice treated with anti-CCR2 (Supplemental Fig. 3B). BAL fluid also showed a reduction in active TGF-β1 in mice with established fibrosis exposed to $PM_{2.5}$ and treated with anti-CCR2 (Supplemental Fig. 3C).

Exposure to $PM_{2.5}$ increased the number of Ly6C^{hi} monocytes in the bone marrow; however, mice receiving anti-CCR2 showed an even greater increase in Ly6C^{hi} monocytes after $PM_{2.5}$ exposure (Supplemental Fig. 3D). Mice treated with IgG control showed Ly6C^{hi} monocytes egress from the bone marrow into the circulation in response to $PM_{2.5}$ exposure, and significantly greater numbers of

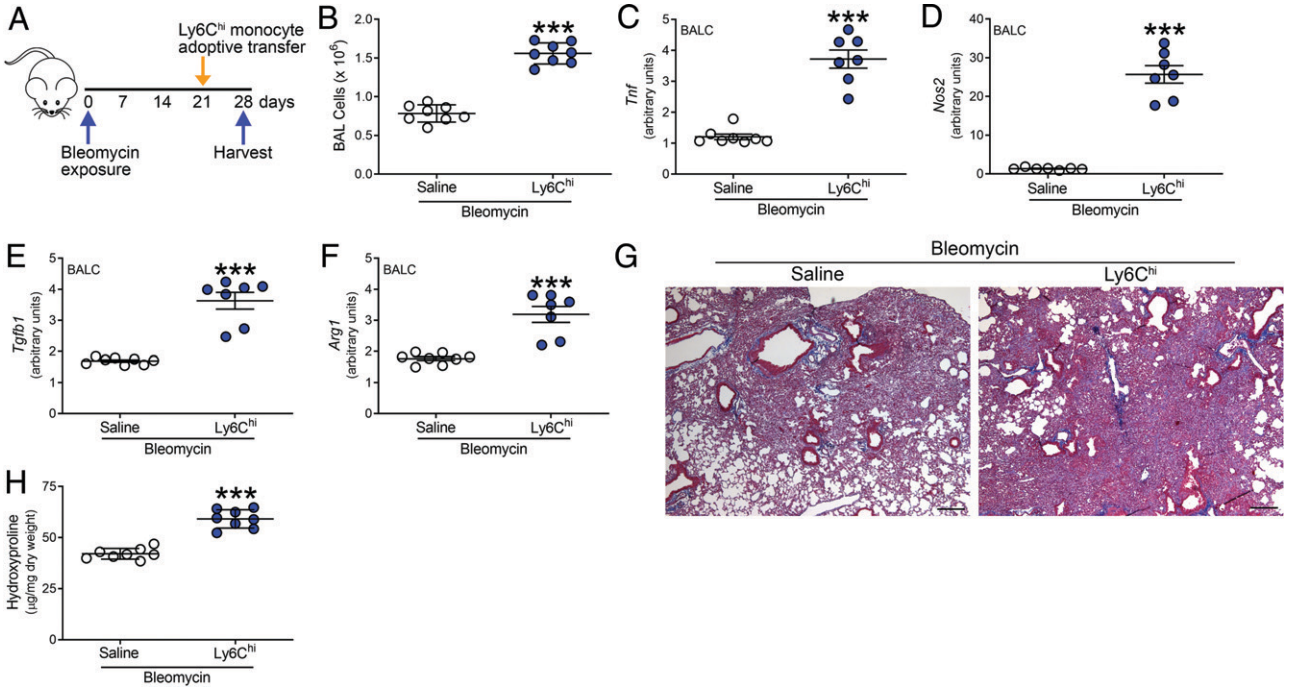

FIGURE 5. Ly6C^{hi} monocytes mediate fibrotic progression in mice with advanced fibrosis. (**A**) Schematic indicating Ly6C^{hi} monocytes derived from bone marrow (1×10^6) were adoptively transferred i.t. into bleomycin-exposed WT mice 21 days after exposure. (**B**) Total number of BAL cells. $n = 8$. mRNA expression in BAL cells for (**C**) *Tnf*, (**D**) *Nos2*, (**E**) *Tgfb1*, and (**F**) *Arg1*. $n = 7–8$. (**G**) Representative Masson's trichrome staining of lung tissues. $n = 7$. Scale bars, 250 μm. (**H**) Hydroxyproline analysis of lung homogenates. $n = 8$. Data shown are representative from two independent experiments. Values shown represent means ± SEM. Two-tailed *t* test statistical analysis was used. ***$p < 0.0001$.

Ly6C^{hi} monocytes were seen in the blood from bleomycin-injured mice with AE-PF (Supplemental Fig. 3E). Despite elevated Ly6C^{hi} monocytes in the bone marrow, mice treated with anti-CCR2 had reduced circulating Ly6C^{hi} monocytes similar to IgG saline controls.

Inhibiting recruitment of Ly6C^{hi} monocytes did not alter normal lung architecture, but there was reduced cellular inflammation in saline-exposed mice receiving $PM_{2.5}$ (Fig. 6H). Although collagen deposition occurred in bleomycin-exposed mice treated with anti-CCR2, the extent of fibrosis was dramatically reduced in bleomycin-injured mice that received $PM_{2.5}$ and anti-CCR2 compared with IgG-treated mice. These histological observations were verified with hydroxyproline analysis (Fig. 6I). The recruitment of Ly6C^{hi} monocytes was associated with restrictive physiology. Bleomycin-injured mice with AE-PF showed a significant reduction in lung compliance compared with bleomycin-injured mice that received vehicle (Fig. 6J). In addition to inhibiting fibrotic progression, anti-CCR2 treatment reduced the restrictive physiology in mice with established fibrosis exposed to $PM_{2.5}$ compared with IgG control mice. Taken together, these observations suggest that therapies to prevent recruitment of classical proinflammatory monocytes may be a novel therapeutic modality to halt AE-IPF.

Discussion

The natural history of IPF is highly variable, and the disease course is difficult to predict (8). AEs are the primary cause of mortality in IPF (11) because a single exacerbation increases the risk of death 10-fold (43). The etiology of AEs is poorly understood; however, potential triggers include infection, aspiration, drug toxicity, or procedure/operation (7). Data indicate that AE-IPF is more common in individuals with advanced fibrosis. Lower baseline lung function, especially reduced forced vital capacity, has been associated with the increased risk for AE-IPF (8). Extensive disease on high-resolution CT and a history of prior AE-IPF also increase the risk of AE (16, 44). Our data showed that AE-PF occurs in mice with advanced fibrosis compared with mice in the early stage of fibrosis, which correlates clinically because AEs occur in individuals with advanced interstitial lung disease (8).

$PM_{2.5}$ exposure contributes to mortality (45), and elevated levels of air pollution are associated with respiratory disease progression in individuals with COPD, asthma, and lung cancer (46). Moreover, exposure to increased levels of air pollution is associated with AE-IPF (12, 13, 15, 16, 18, 35). In addition to $PM_{2.5}$, prior studies show that ozone and nitrogen dioxide are also associated with AE-IPF (12, 16). The $PM_{2.5}$ constituents sulfate, ammonium, and black carbon were associated with rapid disease progression and higher mortality in patients with interstitial lung disease (47). These $PM_{2.5}$ constituents correlated with increased global DNA methylation in peripheral blood samples from IPF subjects with the highest $PM_{2.5}$ exposure (48). Ultrafine particles originating from combustion sources contain sulfur and metals that may mediate the increased risk of respiratory mortality after exposure (49, 50). Although we did not evaluate specific constituents of $PM_{2.5}$, our studies suggest that metals in $PM_{2.5}$ contribute, in part, to the increased oxidative stress seen in our mouse model of AE-PF.

Cytokine expression in plasma and BAL cells strongly suggests cellular heterogeneity in AE-IPF disease. Cultured AE-IPF BAL cells showed increased secretion of CCL2 compared with stable IPF, signifying there is increased monocyte recruitment in AE-IPF (51). Although the proinflammatory cytokines IL-8 and CXCL1 were induced, cultured BAL cells showed a significant increase in cytokine secretion associated with anti-inflammatory and wound healing processes in AE-IPF compared with stable IPF patients (51). In contrast, other studies have identified an exaggerated inflammatory response occurs with elevated IL-6 and C-reactive protein and reduced chitinase 3-like 1 levels (8, 52, 53) in plasma from AE-IPF subjects.

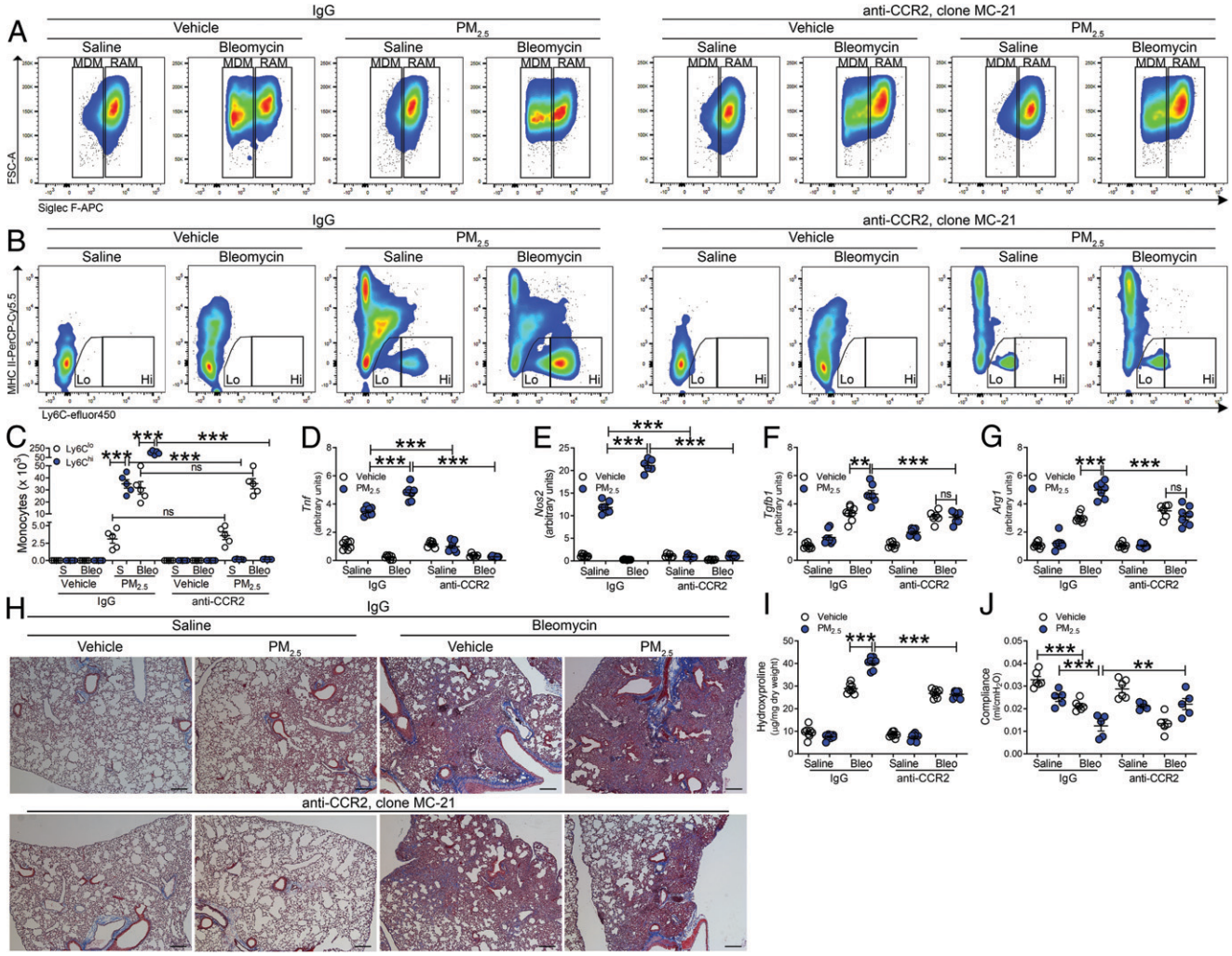

FIGURE 6. Ly6C^{hi} monocytes are required for AE-PF. WT mice were exposed to saline or bleomycin. At day 21, mice were exposed to vehicle or $PM_{2.5}$ daily. On day 23, mice were administered IgG control or anti-CCR2, clone MC-21 Ab (20 μg, i.p. daily). BAL was performed on day 28. Representative flow cytometry plots of (**A**) RAMs and MDMs and (**B**) Ly6C^{lo} and Ly6C^{hi} monocytes. (**C**) Total cell number of Ly6C^{lo} and Ly6C^{hi} monocytes from BAL. $n = 5$. mRNA expression for (**D**) *Tnf*, (**E**) *Nos2*, (**F**) *Tgfb1*, and (**G**) *Arg1* in BAL cells. $n = 4–5$. (**H**) Representative Masson's trichrome staining of lung tissues. $n = 5$. Scale bars, 250 μm. (**I**) Hydroxyproline analysis of lung homogenates. $n = 8$. Data shown were pooled from two independent experiments. (**J**) Compliance was determined by respiratory mechanics analysis. $n = 5–6$. Values shown represent means ± SEM. One-way ANOVA followed by Tukey's multiple comparison test was used. $^{**}p < 0.001$, $^{***}p < 0.0001$. ns, not significant.

Deposition of $PM_{2.5}$ in the alveoli has long been associated with alveolar inflammation and systemic inflammatory response (42), which is seen in exacerbations of asthma and COPD (54). Although previous findings indicate that macrophages have an anti-inflammatory phenotype in several models of pulmonary fibrosis, including IPF (22–27), our data support that an inflammatory response occurs in IPF BAL cells exposed ex vivo to $PM_{2.5}$. We also identified that an inflammatory response occurs in fibrotic mice with AE-PF. Because our results also identified an increased anti-inflammatory response in isolated BAL cells, the mixed heterogeneity of cells in the BAL may contribute to the proinflammatory and anti-inflammatory response that occurs in AE-IPF subjects.

$PM_{2.5}$ exposure has been previously reported to promote monocyte recruitment. Although the Ly6C^{hi} subset has been shown to be present in blood from $PM_{2.5}$-exposed mice, the role these cells play and their presence in the lung in response to $PM_{2.5}$ exposure have not been described (55). A study using adoptive transfer of Ly6C^{hi} bone marrow–derived monocytes into bleomycin-injured mice during the progressive phase of pulmonary fibrosis showed exacerbation of pulmonary fibrosis (56). The increased fibrosis seen by the adoptive transfer of Ly6C^{hi} in mice correlated with an increase in anti-inflammatory lung macrophages; however, the anti-inflammatory lung macrophages were host derived and not from the donor Ly6C^{hi} population. Our data also support that recruited Ly6C^{hi} monocytes exacerbate established fibrosis, and we extend these findings by determining the recruited Ly6C^{hi} monocytes exert an inflammatory response to mediate fibrotic progression. Administration of anti-CCR2 Ab inhibited Ly6C^{hi} monocyte recruitment in $PM_{2.5}$-exposed mice; however, we determined the number of MDMs was also reduced in bleomycin-exposed mice receiving the CCR2 Ab. This agrees with prior evidence that depletion of circulating monocytes using CCR2$^{-/-}$ mice reduced fibrosis severity (22). This also may explain the reduction in anti-inflammatory mediators in the BAL, because the number of Ly6C^{lo} monocytes was not affected. In aggregate, our observations suggest that recruitment of Ly6C^{hi} monocytes in mice exacerbates established pulmonary fibrosis providing a potential mechanism by which elevated $PM_{2.5}$ levels are associated with AE-IPF. Furthermore, we identified that inflammatory classical monocyte recruitment is a potential novel therapeutic target to protect against AE-IPF.

Disclosures

The authors have no financial conflicts of interest.

References

1. Landrigan, P. J., R. Fuller, N. J. R. Acosta, O. Adeyi, R. Arnold, N. N. Basu, A. B. Baldé, R. Bertollini, S. Bose-O'Reilly, J. I. Boufford, et al. 2018. The Lancet Commission on pollution and health. *Lancet* 391: 462–512.
2. Vohra, K., A. Vodonos, J. Schwartz, E. A. Marais, M. P. Sulprizio, and L. J. Mickley. 2021. Global mortality from outdoor fine particle pollution generated by fossil fuel combustion: results from GEOS-Chem. *Environ. Res.* 195: 110754.
3. Fann, N., A. D. Lamson, S. C. Anenberg, K. Wesson, D. Risley, and B. J. Hubbell. 2012. Estimating the national public health burden associated with exposure to ambient PM2.5 and ozone. *Risk Anal.* 32: 81–95.
4. Laden, F., J. Schwartz, F. E. Speizer, and D. W. Dockery. 2006. Reduction in fine particulate air pollution and mortality: extended follow-up of the Harvard Six Cities study. *Am. J. Respir. Crit. Care Med.* 173: 667–672.
5. Harari, S., G. Raghu, A. Caminati, M. Cruciani, M. Franchini, and P. Mannucci. 2020. Fibrotic interstitial lung diseases and air pollution: a systematic literature review. *Eur. Respir. Rev.* 29: 200093.
6. Sack, C., and G. Raghu. 2019. Idiopathic pulmonary fibrosis: unmasking cryptogenic environmental factors. *Eur. Respir. J.* 53: 1801699.
7. Raghu, G., M. Remy-Jardin, J. L. Myers, L. Richeldi, C. J. Ryerson, D. J. Lederer, J. Behr, V. Cottin, S. K. Danoff, F. Morell, et al.; American Thoracic Society; European Respiratory Society; Japanese Respiratory Society; and Latin American Thoracic Society. 2018. Diagnosis of idiopathic pulmonary fibrosis. An official ATS/ERS/JRS/ALAT Clinical Practice Guideline. *Am. J. Respir. Crit. Care Med.* 198: e44–e68.
8. Song, J. W., S. B. Hong, C. M. Lim, Y. Koh, and D. S. Kim. 2011. Acute exacerbation of idiopathic pulmonary fibrosis: incidence, risk factors and outcome. *Eur. Respir. J.* 37: 356–363.
9. Kim, D. S., J. H. Park, B. K. Park, J. S. Lee, A. G. Nicholson, and T. Colby. 2006. Acute exacerbation of idiopathic pulmonary fibrosis: frequency and clinical features. *Eur. Respir. J.* 27: 143–150.
10. Ryerson, C. J., V. Cottin, K. K. Brown, and H. R. Collard. 2015. Acute exacerbation of idiopathic pulmonary fibrosis: shifting the paradigm. *Eur. Respir. J.* 46: 512–520.
11. Collard, H. R., C. J. Ryerson, T. J. Corte, G. Jenkins, Y. Kondoh, D. J. Lederer, J. S. Lee, T. M. Maher, A. U. Wells, K. M. Antoniou, et al. 2016. Acute exacerbation of idiopathic pulmonary fibrosis. An International Working Group Report. *Am. J. Respir. Crit. Care Med.* 194: 265–275.
12. Sesé, L., H. Nunes, V. Cottin, S. Sanyal, M. Didier, Z. Carton, D. Israel-Biet, B. Crestani, J. Cadranel, B. Wallaert, et al. 2018. Role of atmospheric pollution on the natural history of idiopathic pulmonary fibrosis. *Thorax* 73: 145–150.
13. Winterbottom, C. J., R. J. Shah, K. C. Patterson, M. E. Kreider, R. A. Panettieri, Jr., B. Rivera-Lebron, W. T. Miller, L. A. Litzky, T. M. Penning, K. Heinlen, et al. 2018. Exposure to ambient particulate matter is associated with accelerated functional decline in idiopathic pulmonary fibrosis. *Chest* 153: 1221–1228.
14. Rice, M. B., P. L. Ljungman, E. H. Wilker, K. S. Dorans, D. R. Gold, J. Schwartz, P. Koutrakis, G. R. Washko, G. T. O'Connor, and M. A. Mittleman. 2015. Long-term exposure to traffic emissions and fine particulate matter and lung function decline in the Framingham heart study. *Am. J. Respir. Crit. Care Med.* 191: 656–664.
15. Tahara, M., Y. Fujino, K. Yamasaki, K. Oda, T. Kido, N. Sakamoto, T. Kawanami, K. Kataoka, R. Egashira, M. Hashisako, et al. 2021. Exposure to $PM_{2.5}$ is a risk factor for acute exacerbation of surgically diagnosed idiopathic pulmonary fibrosis: a case-control study. *Respir. Res.* 22: 80.
16. Johannson, K. A., E. Vittinghoff, K. Lee, J. R. Balmes, W. Ji, G. G. Kaplan, D. S. Kim, and H. R. Collard. 2014. Acute exacerbation of idiopathic pulmonary fibrosis associated with air pollution exposure. *Eur. Respir. J.* 43: 1124–1131.
17. Dales, R., C. Blanco-Vidal, and S. Cakmak. 2020. The association between air pollution and hospitalization of patients with idiopathic pulmonary fibrosis in Chile: a daily time series analysis. *Chest* 158: 630–636.
18. Johannson, K. A., E. Vittinghoff, J. Morisset, P. J. Wolters, E. M. Noth, J. R. Balmes, and H. R. Collard. 2018. Air pollution exposure is associated with lower lung function, but not changes in lung function, in patients with idiopathic pulmonary fibrosis. *Chest* 154: 119–125.
19. Scott, M. K. D., K. Quinn, Q. Li, R. Carroll, H. Warsinske, F. Vallania, S. Chen, M. A. Carns, K. Aren, J. Sun, et al. 2019. Increased monocyte count as a cellular biomarker for poor outcomes in fibrotic diseases: a retrospective, multicentre cohort study. *Lancet Respir. Med.* 7: 497–508.
20. Kreuter, M., J. S. Lee, A. Tzouvelekis, J. M. Oldham, P. L. Molyneaux, D. Weycker, M. Atwood, K. U. Kirchgaessler, and T. M. Maher. 2021. Monocyte count as a prognostic biomarker in patients with idiopathic pulmonary fibrosis. *Am. J. Respir. Crit. Care Med.* 204: 74–81.
21. Kawamura, K., K. Ichikado, K. Anan, Y. Yasuda, Y. Sekido, M. Suga, H. Ichiyasu, and T. Sakagami. 2020. Monocyte count and the risk for acute exacerbation of fibrosing interstitial lung disease: a retrospective cohort study. *Chron. Respir. Dis.* 17: 1479973120909840.
22. Larson-Casey, J. L., M. Vaid, L. Gu, C. He, G. Q. Cai, Q. Ding, D. Davis, T. F. Berryhill, L. S. Wilson, S. Barnes, et al. 2019. Increased flux through the mevalonate pathway mediates fibrotic repair without injury. *J. Clin. Invest.* 129: 4962–4978.
23. Larson-Casey, J. L., J. S. Deshane, A. J. Ryan, V. J. Thannickal, and A. B. Carter. 2016. Macrophage Akt1 kinase-mediated mitophagy modulates apoptosis resistance and pulmonary fibrosis. *Immunity* 44: 582–596.
24. Gu, L., J. L. Larson-Casey, and A. B. Carter. 2017. Macrophages utilize the mitochondrial calcium uniporter for profibrotic polarization. *FASEB J.* 31: 3072–3083.
25. Larson-Casey, J. L., C. He, P. Che, M. Wang, G. Cai, Y. I. Kim, M. El Hamdaoui, R. Grytz, Q. Ding, and A. B. Carter. 2020. Technical advance: the use of tree shrews as a model of pulmonary fibrosis. *PLoS One* 15: e0241323.
26. He, C., J. L. Larson-Casey, D. Davis, V. S. Hanumanthu, A. L. F. Longhini, V. J. Thannickal, L. Gu, and A. B. Carter. 2019. NOX4 modulates macrophage phenotype and mitochondrial biogenesis in asbestosis. *JCI Insight* 4: e126551.
27. Murthy, S., J. L. Larson-Casey, A. J. Ryan, C. He, L. Kobzik, and A. B. Carter. 2015. Alternative activation of macrophages and pulmonary fibrosis are modulated by scavenger receptor, macrophage receptor with collagenous structure. *FASEB J.* 29: 3527–3536.
28. Kreuter, M., M. Polke, S. L. F. Walsh, J. Krisam, H. R. Collard, N. Chaudhuri, S. Avdeev, J. Behr, G. Calligaro, T. Corte, et al. 2020. Acute exacerbation of idiopathic pulmonary fibrosis: international survey and call for harmonisation. *Eur. Respir. J.* 55: 1901760.
29. He, C., S. Murthy, M. L. McCormick, D. R. Spitz, A. J. Ryan, and A. B. Carter. 2011. Mitochondrial Cu,Zn-superoxide dismutase mediates pulmonary fibrosis by augmenting H2O2 generation. *J. Biol. Chem.* 286: 15597–15607.
30. Gavett, S. H., N. Haykal-Coates, J. W. Highfill, A. D. Ledbetter, L. C. Chen, M. D. Cohen, J. R. Harkema, J. G. Wagner, and D. L. Costa. 2003. World Trade Center fine particulate matter causes respiratory tract hyperresponsiveness in mice. *Environ. Health Perspect.* 111: 981–991.
31. Mack, M., J. Cihak, C. Simonis, B. Luckow, A. E. Proudfoot, J. Plachý, H. Brühl, M. Frink, H. J. Anders, V. Vielhauer, et al. 2001. Expression and characterization of the chemokine receptors CCR2 and CCR5 in mice. *J. Immunol.* 166: 4697–4704.
32. Fedorov, A., R. Beichel, J. Kalpathy-Cramer, J. Finet, J. C. Fillion-Robin, S. Pujol, C. Bauer, D. Jennings, F. Fennessy, M. Sonka, et al. 2012. 3D Slicer as an image computing platform for the Quantitative Imaging Network. *Magn. Reson. Imaging* 30: 1323–1341.
33. De Langhe, E., G. Vande Velde, J. Hostens, U. Himmelreich, B. Nemery, F. P. Luyten, J. Vanoirbeek, and R. J. Lories. 2012. Quantification of lung fibrosis and emphysema in mice using automated micro-computed tomography. *PLoS One* 7: e43123.
34. Gu, L., R. Surolia, J. L. Larson-Casey, C. He, D. Davis, J. Kang, V. B. Antony, and A. B. Carter. 2022. Targeting Cpt1a-Bcl-2 interaction modulates apoptosis resistance and fibrotic remodeling. *Cell Death Differ.* 29: 118–132.
35. Tomos, I., K. Dimakopoulou, E. D. Manali, S. A. Papiris, and A. Karakatsani. 2021. Long-term personal air pollution exposure and risk for acute exacerbation of idiopathic pulmonary fibrosis. *Environ. Health* 20: 99.
36. Larson-Casey, J. L., L. Gu, D. Davis, G. Q. Cai, Q. Ding, C. He, and A. B. Carter. 2021. Post-translational regulation of PGC-1α modulates fibrotic repair. *FASEB J.* 35: e21675.
37. McCubbrey, A. L., L. Barthel, M. P. Mohning, E. F. Redente, K. J. Mould, S. M. Thomas, S. M. Leach, T. Danhorn, S. L. Gibbings, C. V. Jakubzick, et al. 2018. Deletion of c-FLIP from $CD11b^{hi}$ macrophages prevents development of bleomycin-induced lung fibrosis. *Am. J. Respir. Cell Mol. Biol.* 58: 66–78.
38. Redente, E. F., R. C. Keith, W. Janssen, P. M. Henson, L. A. Ortiz, G. P. Downey, D. L. Bratton, and D. W. Riches. 2014. Tumor necrosis factor-α accelerates the resolution of established pulmonary fibrosis in mice by targeting profibrotic lung macrophages. *Am. J. Respir. Cell Mol. Biol.* 50: 825–837.
39. Misharin, A. V., L. Morales-Nebreda, P. A. Reyfman, C. M. Cuda, J. M. Walter, A. C. McQuattie-Pimentel, C. I. Chen, K. R. Anekalla, N. Joshi, K. J. N. Williams, et al. 2017. Monocyte-derived alveolar macrophages drive lung fibrosis and persist in the lung over the life span. *J. Exp. Med.* 214: 2387–2404.
40. Guilliams, M., A. Mildner, and S. Yona. 2018. Developmental and functional heterogeneity of monocytes. *Immunity* 49: 595–613.
41. Larson-Casey, J. L., L. Gu, O. Fiehn, and A. B. Carter. 2020. Cadmium-mediated lung injury is exacerbated by the persistence of classically activated macrophages. *J. Biol. Chem.* 295: 15754–15766.
42. Spengler, J. D., and G. D. Thurston. 1983. Mass and elemental composition of fine and coarse particles in six U.S. cities. *J. Air Pollut. Control Assoc.* 33: 1162–1171.
43. Paterniti, M. O., Y. Bi, D. Rekić, Y. Wang, B. A. Karimi-Shah, and B. A. Chowdhury. 2017. Acute exacerbation and decline in forced vital capacity are associated with increased mortality in idiopathic pulmonary fibrosis. *Ann. Am. Thorac. Soc.* 14: 1395–1402.
44. Kishaba, T., H. Tamaki, Y. Shimaoka, H. Fukuyama, and S. Yamashiro. 2014. Staging of acute exacerbation in patients with idiopathic pulmonary fibrosis. *Lung* 192: 141–149.
45. Dockery, D. W., C. A. Pope III, X. Xu, J. D. Spengler, J. H. Ware, M. E. Fay, B. G. Ferris, Jr., and F. E. Speizer. 1993. An association between air pollution and mortality in six U.S. cities. *N. Engl. J. Med.* 329: 1753–1759.
46. Wang, X., L. Chen, M. Cai, F. Tian, H. Zou, Z. M. Qian, Z. Zhang, H. Li, C. Wang, S. W. Howard, et al. 2023. Air pollution associated with incidence and progression trajectory of chronic lung diseases: a population-based cohort study. *Thorax* 78: 698–705.
47. Goobie, G. C., C. Carlsten, K. A. Johannson, N. Khalil, V. Marcoux, D. Assayag, H. Manganas, J. H. Fisher, M. R. J. Kolb, K. O. Lindell, et al. 2022. Association of particulate matter exposure with lung function and mortality among patients with fibrotic interstitial lung disease. *JAMA Intern. Med.* 182: 1248–1259.
48. Goobie, G. C., X. Li, C. J. Ryerson, C. Carlsten, K. A. Johannson, J. P. Fabisiak, K. O. Lindell, X. Chen, K. F. Gibson, D. J. Kass, et al. 2023. $PM_{2.5}$ and constituent component impacts on global DNA methylation in patients with idiopathic pulmonary fibrosis. *Environ. Pollut.* 318: 120942.
49. Schwarz, M., A. Schneider, J. Cyrys, S. Bastian, S. Breitner, and A. Peters. 2023. Impact of ambient ultrafine particles on cause-specific mortality in three German cities. *Am. J. Respir. Crit. Care Med.* 207: 1334–1344.

50. Pope III, C. A., M. Ezzati, and D. W. Dockery. 2009. Fine-particulate air pollution and life expectancy in the United States. *N. Engl. J. Med.* 360: 376–386.
51. Schupp, J. C., H. Binder, B. Jäger, G. Cillis, G. Zissel, J. Müller-Quernheim, and A. Prasse. 2015. Macrophage activation in acute exacerbation of idiopathic pulmonary fibrosis. *PLoS One* 10: e0116775.
52. Collard, H. R., C. S. Calfee, P. J. Wolters, J. W. Song, S. B. Hong, S. Brady, A. Ishizaka, K. D. Jones, T. E. King, Jr., M. A. Matthay, and D. S. Kim. 2010. Plasma biomarker profiles in acute exacerbation of idiopathic pulmonary fibrosis. *Am. J. Physiol. Lung Cell. Mol. Physiol.* 299: L3–L7.
53. Zhou, Y., H. Peng, H. Sun, X. Peng, C. Tang, Y. Gan, X. Chen, A. Mathur, B. Hu, M. D. Slade, et al. 2014. Chitinase 3-like 1 suppresses injury and promotes fibroproliferative responses in Mammalian lung fibrosis. *Sci. Transl. Med.* 6: 240ra76.
54. Aghapour, M., N. D. Ubags, D. Bruder, P. S. Hiemstra, V. Sidhaye, F. Rezaee, and I. H. Heijink. 2022. Role of air pollutants in airway epithelial barrier dysfunction in asthma and COPD. *Eur. Respir. Rev.* 31: 210112.
55. Gangwar, R. S., V. Vinayachandran, P. Rengasamy, R. Chan, B. Park, R. Diamond-Zaluski, E. A. Cara, A. Cha, L. Das, C. Asase, et al. 2020. Differential contribution of bone marrow-derived infiltrating monocytes and resident macrophages to persistent lung inflammation in chronic air pollution exposure. *Sci. Rep.* 10: 14348.
56. Gibbons, M. A., A. C. MacKinnon, P. Ramachandran, K. Dhaliwal, R. Duffin, A. T. Phythian-Adams, N. van Rooijen, C. Haslett, S. E. Howie, A. J. Simpson, et al. 2011. Ly6Chi monocytes direct alternatively activated profibrotic macrophage regulation of lung fibrosis. *Am. J. Respir. Crit. Care Med.* 184: 569–581.